Near-infrared afterglow semiconducting nano-polycomplexes for multiplex differentiation of cancer exosomes

Lyu, Yan; Cui, Dong; Huang, Jiaguo; Fan, Wenxuan; Miao, Yansong; Pu, Kanyi

2019

Lyu, Y., Cui, D., Huang, J., Fan, W., Miao, Y., & Pu, K. (2019). Near-infrared afterglow semiconducting nano-polycomplexes for the multiplex differentiation of cancer exosomes. Angewandte Chemie International Edition, 58(15), 4983-4987. doi:10.1002/anie.201900092

https://hdl.handle.net/10356/82615

https://doi.org/10.1002/anie.201900092

COMMUNICATION

Near-Infrared Afterglow Semiconducting Nano-polycomplexes for Multiplex Differentiation of Cancer Exosomes

Yan Lyu,[a] Dong Cui,[a] Jiaguo Huang,[a] Wenxuan Fan,[a] Yansong Miao[a,b] and Kanyi Pu*[a]

Abstract: As nanoscaled extracellular vehicles inheriting genetic and protein information from source cells, detection of exosomes is promising for early diagnosis of cancer. However, optical sensors with high specificity and low medium background remain challenging for detection of exosomes. We herein develop the first luminescent nanosensor that bypasses real-time light excitation for multiplex differentiation of cancer exosomes. Such an afterglow luminescent nanosensor is composed of a near-infrared (NIR) semiconducting polyelectrolyte (ASPN) electrostatically complexed with a quencher-tagged aptamer. The afterglow signal of the nanocomplex (ASPNC) is initially quenched due to the efficient electron transfer between ASPN and the quencher. However, the presence of aptamer-targeted exosome increases ASPN/quencher distance, turning on afterglow signal. Because the afterglow detection is conducted after cessation of light excitation, the sample background signal is greatly minimized, affording the limit of detection that is nearly two orders of magnitude lower than fluorescence detection in cell culture medium. More importantly, ASPNC can be easily tailored to detect different exosomal proteins simply by changing the sequence of aptamer. Such a structural versatility of ASPNC enables orthogonal analysis of multiple exosome samples, potentially permitting accurate identification of the cellular origin of exosomes for cancer diagnosis.

Exosomes as one of nanoscaled extracellular vehicles play an important role in cell communication and are implicated in the pathogenesis including neurodegenerative diseases,[1] viral/bacterial infections[2] and cancers.[3] Because exosomes carry genetic and protein information inherited from their parent cells and have high stability in circulation, exosomes have been isolated and used to identify the biomarkers for diseases.[3-4] In particular, as compared with circulating tumor cells (CTCs) and serum proteins that have their respective disadvantages of extremely low blood concentration and poor specificity caused by their uncertain origins,[5] exosomes serve as more promising targets in early diagnosis of cancer; moreover, exosomal protein levels are often associated with the disease status and thus can be used to monitor therapeutic responses for precision medicines.[6] Thus, specific detection of cancer exosomes provides new opportunities for cancer diagnosis and therapy.

To analyze the whole set of exosomal bioinformation, molecular sensors are required to differentiate the subtle variation between exosomes derived from cancer and normal cells. In this regard, electrochemical sensors have been exploited,[7] which however have the shortages such as the interference caused by temperature sensitivity and difficulty in multiplex screening.[8] In contrast, optical sensors based on light scattering,[9] absorption[10] or fluorescence[11] avoid those limitations and have the potential for high-throughput detection of exosomes. Among them, fluorescence detection generally has the highest sensitivity and has been integrated with the standard bioassays including Western blot and enzyme-linked immunosorbent assay (ELISA) to detect exosomes through specific binding between antibody and receptor on the surface of exosomes.[11] However, residual biomolecules in the testing samples often cause the background fluorescence signal,[12] which partially compromises the sensitivity and requires additional washing operations before detection.

Semiconducting polymer nanoparticles have emerged as a versatile category of optical materials for molecular imaging and cancer therapy because of their good biocompatibility and high absorption coefficients.[13] Recently, we discovered that poly(phenylenevinylene) (PPV)-based SPNs can emit long-living luminescence even after cessation of light excitation.[14] Such afterglow emission is associated with the photoirradiation-induced production of singlet oxygen ($^1O_2$) which spontaneously reacts with the vinylene bonds of PPV to form dioxetane units. These defect units are unstable and gradually degrade to emit photons as one of the products. Such an excitation-free luminescence process of PPV-based SPNs eliminates the tissue background noise, leading to significantly increased sensitivity for detection of cancer,[14a] lymph nodes and even disease biomarkers in living animals.[14d]

In this study, we synthesize an afterglow semiconducting polyelectrolyte (ASP) and utilize it to construct afterglow semiconducting polyelectrolyte nanocomplex (ASPNC) for specific detection of cancer exosomes. A near-infrared (NIR) $^1O_2$ photosensitizer, tetraphenylporphyrin (TPP), is incorporated into the backbone of PPV to red-shift the emission and amplify the afterglow signal (Figure 1a); whereas, cationic quaternary ammonium groups are attached as the side chains of PPV to form the nanocomplexes with the quencher (BHQ-2: black hole quencher 2)-tagged aptamer through electrostatic attraction (Figure 1b). Because of the efficient electron transfer between the PPV backbone and BHQ-2 within the compact nanocomplexes, both fluorescence and afterglow signals of ASPNC are quenched at the initial state (Figure 1b). However, in the presence of the targeted exosome, the specific binding between aptamer and exosome occurs to increase the PPV/BHQ2 distance, which deters the electron transfer and turns on both fluorescence and afterglow signals. Such an ASPNC design not only allows to specifically detect exosomes secreted from different cells using the corresponding quencher-tagged aptamer but also permits the sensitive optical detection with low background noises because of eliminated real-time light excitation.

[a] Y. Lyu, D. Cui, J. Huang, W. Fan, Prof. Y. Miao, Prof. K. Pu
School of Chemical and Biomedical Engineering
Nanyang Technological University
Singapore, 637457 (Singapore)
E-mail: kypu@ntu.edu.sg
[b] Prof. Y. Miao
School of Biological Science
Nanyang Technological University
Singapore, 637551 (Singapore)

Supporting information for this article is given via a link at the end of the document.

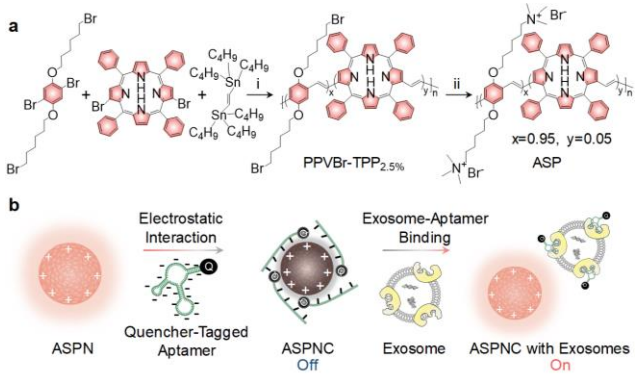

Figure 1. Design and sensing mechanism of ASPNC. (a) Synthetic route of ASP. Reagents and conditions: i) tris(dibenzylideneacetone)dipalladium(0) [$Pd_2(dba)_3$], tri(*p*-tolyl)phosphine (TPTP), chlorobenzene, 100 ºC, 24 h; ii) trimethylamine, tetrahydrofuran (THF), methanol, 24 h. (b) The schematic illustration of formation of ASPNC and afterglow turn-on detection of exosomes.

The synthetic route of ASP was depicted in Figure 1a. The monomer 1,4-dibromo-2,5-bis((6-bromohexyl)oxy)benzene was copolymerized with 7,18-dibromo-5,10,15,20-tetraphenylporphyrin (TPP-Br) and trans-1,2-bis(tributylstannyl)ethene at the molar ratio of 19:1:20 *via* Pd-catalyzed Stille coupling reaction to yield the intermediate polymer, PPVBr-$TPP_{2.5\%}$. The TPP doping amount was chosen at 2.5% because the corresponding polymer had the higher afterglow signals and the better quenching efficacy after complexing with BHQ-2 as compared to the polymers with the lower or higher doping amount (Supporting Information, Figure S1). The final polymer (ASP) was obtained by converting the bromine groups of PPVBr-$TPP_{2.5\%}$ to quaternary ammonium groups, endowing ASP with both the hydrophilicity and positive charges. The chemical structures of monomer 1,4-dibromo-2,5-bis((6-bromohexyl)oxy)benzene, PPVBr-$TPP_{2.5\%}$ and ASP were confirmed by proton nuclear magnetic resonance (^{1}H NMR) analysis (Supporting Information, Figures S2-S4).

ASP could spontaneously assemble into the nanoparticles in aqueous solutions, termed as ASPN. ASPN had the average hydrodynamic diameters of 35 ± 8 nm with a spherical morphology (Figure 2a). After complexing with the BHQ-2-tagged aptamer (Apt_{CD63}) which specifically binds with a ubiquitous exosomal protein CD63, the average size increased to 104±44 nm, along with the decrease of zeta potential from 16.9±1.9 to -19.4±5.1 mV (Figure 2b; Figure S5, Supporting Information). Thus, the increased size and decreased zeta potential confirmed the formation of the nanocomplex (ASPNC).

The optical properties and sensing abilities of ASPNC were tested. ASPN had the absorption ranging from 350 to 550 nm and the maximum emission at ~680 nm (Supporting Information, Figure S6). Due to the good spectral overlap between the emission of ASPN and the absorption of BHQ-2 and their short distance within the nanocomplexes, both fluorescence and afterglow signals of ASPNC were substantially quenched, leading to the relatively low signals (Supporting Information, Figure S7). However, in the presence of the targeted exosomes (Hela secreted exosomes), the afterglow and fluorescence signals of ASPNC at 680 nm increased by 4.69- and 1.84-fold, respectively (Figure 2c, d). Such signal increases of ASPNC were attributed to the increased distance between ASP and BHQ-2 upon the specific binding of Apt_{CD63} with CD63 on the Hela exosomes. Thus, these spectral data verified the sensing mechanism of ASPNC as illustrated in Figure 1b.

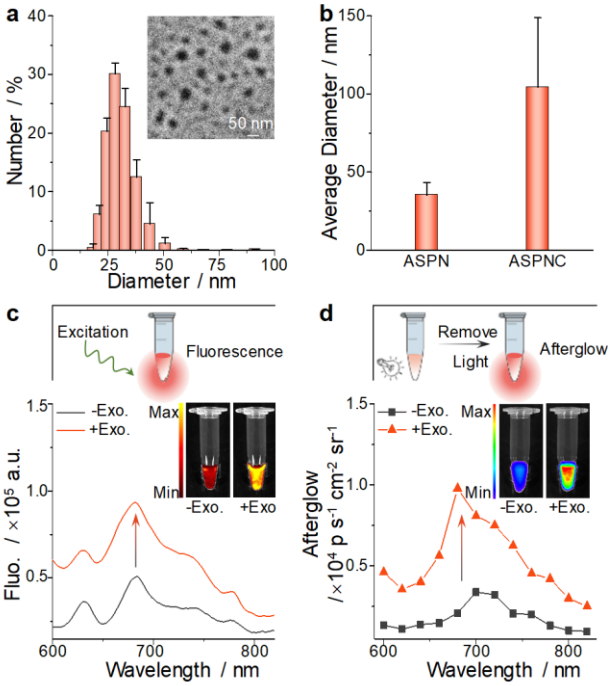

Figure 2. Characterization of ASPNC. (a) Size distribution measured by dynamic light scattering (DLS) of ASPN. Inset: the transmission electron microscope (TEM) image of ASPN. (b) Average hydrodynamic diameters of ASPN and ASPNC. Fluorescence (c) and afterglow (d) spectra of ASPNC with and without exosomes (Exo.). Inset: fluorescence (c) and afterglow (d) images of ASPNC with and without exosomes. [SPN]=10 μg mL^{-1} in PBS buffer. The fluorescence spectra were measured under the excitation of 520 nm. Fluorescence images were acquired for 0.1 s at 680±10 nm upon the excitation at 520±10 nm. Afterglow images were pre-irradiated by white light (0.1 W cm^{-2}) for 10 s and acquired under IVIS bioluminescence after the removal of the light source. Error bars were based on the standard deviations (SD) of three parallel samples.

To verify the advantage of afterglow over fluorescence, detection of the Hela secreted exosomes was conducted in different media. The signal recovery ratio was defined as the signal increase of ASPNC with the presence of exosomes divided by the signal difference between ASPN and ASPNC. In all testing solutions, the signal recovery ratios of both afterglow and fluorescence increased with the increase of exosomes (Figure 3a-c). However, the signal recovery ratios of afterglow were always higher than those of fluorescence at the same exosome concentration, proving the higher sensitivity of afterglow. Such a difference became more significant when changing the media from PBS to mouse plasma and complete culture medium containing 10% fetal bovine serum (FBS). In particular, the afterglow detection had the limit of detection (LOD) values lower than those of fluorescence in all testing solutions. Note that in PBS buffer, ASPNC had the limit of detection (0.24 μg mL^{-1}), which was comparable or lower than the reported sensors.[7-11] However, when changing the detection medium from PBS to plasma or to cell culture medium, the afterglow LOD remained

almost unchanged, but the fluorescence LOD dramatically increased (Figure 3d). There, the afterglow LOD was 3.0, 6.9, and 93-fold lower than the fluorescence LOD in PBS, plasma and complete cell culture medium, respectively.

To figure out the higher sensitivity of afterglow over fluorescence, the backgrounds (BKGs) of afterglow or fluorescence signals of all testing media were measured and normalized to those of PBS buffer (Figure 3d). It was found that the fluorescence BKG signals of plasma and culture medium were 5.5- and 36.0-fold higher than that of PBS buffer, respectively; while the afterglow BKG signals in those media remained as low as that in PBS buffer (PBS:1.0; plasma: 1.0, medium: 1.3). The strong autofluorescence signals in plasma and culture medium should be attributed to the fact that emissive biomolecules, such as hemoglobin, flavin and lipofuscin,[12] are present. Such signal interference was avoided by afterglow because the detection was conducted without real-time light excitation. As plasma and culture medium are more relevant to blood than PBS, these data implied that ASPNC-based afterglow detection could potentially require less purification steps for testing exosome samples.

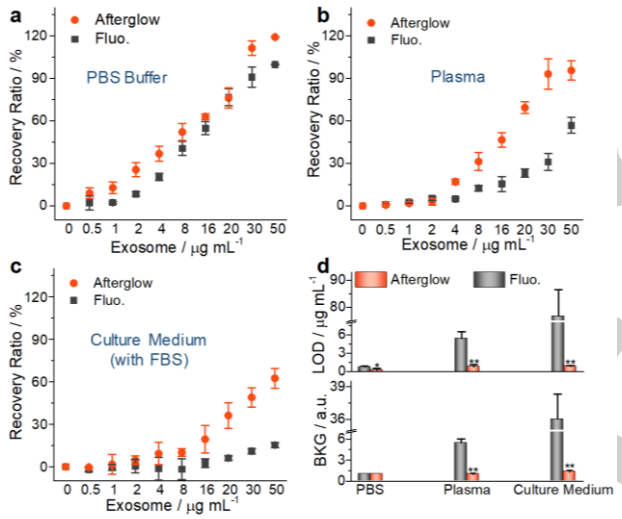

Figure 3. Exosomes detection in different testing media using ASPNC. The signal recovery ratios of afterglow and fluorescence of ASPNC as a function of exosome concentrations detected in PBS buffer (pH 7.4) (a), mouse plasma (b) or complete culture medium (containing 10% FBS) (c). (d) The limit of detection (LOD) values and the background (BKG) signals determined by afterglow and fluorescence (Fluo.) in PBS buffer, mouse plasma or complete culture medium. Error bars were based on the standard deviations (SD) of three samples. Statistically significant differences existed in LODs/BKG signals determined by afterglow and fluorescence in PBS buffer, mouse plasma and complete culture medium (*p<0.05, **p<0.01).

It is well known that exosomes carry proteins and nucleic acids related to the types and corresponding metabolic status of parent cells (Figure 4a).[15] Such exosomal information can be considered as the 'fingerprint' of its parent cells and potentially used for identification of cancer cells. To test the recognition ability of ASPNC-based afterglow sensors, five kinds of exosomes secreted from Hela (cervical cancer cells), chondrocytes (benign cells), MCF-7 (breast cancer cells), SKOV3 (ovarian cancer cells) and HepG2 (liver cancer cells) were orthogonally examined in terms of expression levels of four different biomarkers including CD63, the epithelial cell adhesion molecule (EpCAM), human epidermal growth factor receptor 2 (HER2) and mucin1 (MUC1). The binding specificity of ASPNC was mediated by using different BHQ-2-tagged aptamers, which included Apt_{CD63}, Apt_{EpCAM}, Apt_{HER2} and Apt_{MUC1} (Supporting Information, Table S1) for CD63, EpCAM, HER2 and MUC1, respectively. The exosomal protein levels were determined by the afterglow recovery ratio per unit concentration of exosomes and summarized as the heat map in Figure 4b. It was obvious that the four biomarkers existed in all five exosomes with different amounts. Among them, MCF7-secreted exosomes expressed the highest levels of MUC1, HER2 and EpCAM; while the highest expression level of CD63 was found in Hela-secreted exosomes. These findings were consistent with the previous reports, showing the dramatically upregulated transcription level of cellular MUC1 in MCF-7[16] and exosomal CD63 in Hela.[10b] These data also verified the capability of ASPNC to differentiate the subtle variation of protein levels in exosomes from different source cells.

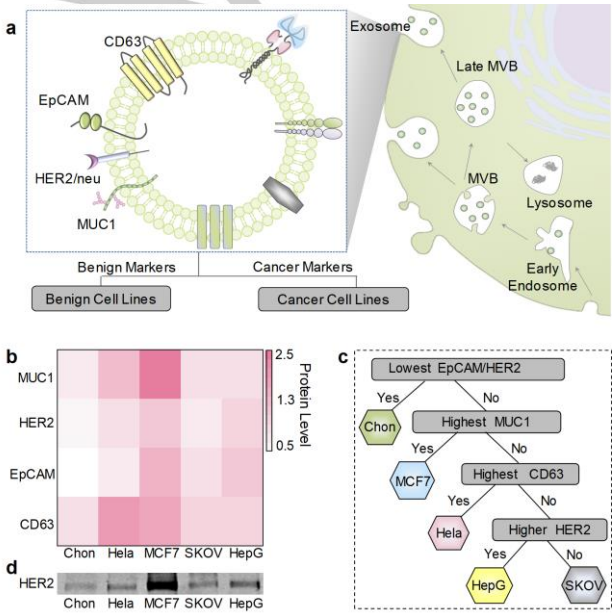

Figure 4. Differentiation of cancer exosomes using ASPNC. (a) Schematic illustration of the origin of exosomes possessing different biomarkers. (b) Heat map indicating the expression levels of four different biomarkers (CD63, EpCAM, HER2, MUC1) of exosomes from five different cell lines (Chondrocyte, Hela, MCF-7, SKOV3 and HepG2). The biomarker levels were indicated by the afterglow recovery ratio per unit concentration of exosomes. (c) Proof-of-concept demonstration of distinguishing benign or cancer cell secreted exosomes according to Figure 4(b). (d) Representative Western blot analysis of HER2 expression in the five cell lines. The total protein amounts for each sample in Western blot were the same. Chon, SKOV and HepG indicated chondrocyte, SKOV3 and HepG2 cell lines, respectively.

As a proof-of-concept, the panel of exosomal protein information was attempted to identify the source cells of exosomes (Figure 4c). Because EpCAM and HER2 were proved to be the cancer biomarkers,[10a] their exosomal levels served as the first criterion to distinguish cancer cells from normal cells (Figure 4c). Then, other exosomal biomarkers could be used to further identify cancer cell lines. For instance, the highest level of exosomal MUC1 and CD63 distinguished MCF-7-secreted and

Hela-secreted exosomes from the others, respectively. At last, HepG2-secreted exosome was differentiated itself from SKOV3-secreted exosome by its higher exosomal HER2 which was also confirmed by Western blot analysis (Figure 4d; Supporting Information, Figure S8). Consequently, ASPNC-based orthogonal detection of four biomarkers was able to distinguish exosomes secreted from five different cells.

In conclusion, we have synthesized a NIR afterglow polymer (ASPN) and assembled it with the quencher-tagged aptamer to form the nanocomplex (ASPNC) for specific detection of cancer exosomes. ASPNC-based afterglow sensor had the minimized signal background from sample media owing to the elimination of real-time excitation during optical detection. Such a unique advantage of afterglow detection led to the LOD of exosomes that was almost two orders of magnitude (93-fold) lower than that for fluorescence detection when conducting in cell culture medium. By varying the sequence of aptamer used in the nanocomplex, ASPNC was able to specifically detect different exosomal protein biomarkers. Such a structural diversity allowed ASPNC to serve as a platform to perform orthogonal analysis of multiple exosome samples, potentially allowing for accurate identification of the source cells for exosomes. To the best of our knowledge, ASPNC represents the first optical sensor that does not require real-time light excitation for detection of exosomes. In view of its background minimized feature, ASPNC-based exosome sensor is promising for high-through and sensitive multiplex protein profiling of exosomes with simplified sample processing. However, such a nanosensor requires careful selection of appropriate aptamers which play crucial role in its specificity and sensitivity.

Acknowledgements

K.P. thanks the finical support from Nanyang Technological University (Start-Up grant: NTU-SUG: M4081627.120) and Singapore Ministry of Education Academic Research Fund Tier1 (RG133/15 M4011559, 2017-T1-002-134-RG147/17) and Tier 2 (MOE2016-T2-1-098 & MOE2018-T2-2-042). Y.M. thanks Singapore Ministry of Education Academic Research Fund Tier 2 (MOE2016-T2-1-005(S)).

Conflict of Interest

The authors declare no conflict of interest.

Keywords: biosensor • nanomaterials • semiconducting polymer • optical imaging • exosome

[1] J. Brettschneider, K. Del Tredici, V. M. Y. Lee, J. Q. Trojanowski, *Nat. Rev. Neurosci.* **2015**, *16*, 109-120.
[2] J. S. Schorey, C. V. Harding, *J. Clin. Invest.* **2016**, *126*, 1181-1189.
[3] R. Xu, A. Rai, M. S. Chen, W. Suwakulsiri, D. W. Greening, R. J. Simpson, *Nat. Rev. Clin. Oncol.* **2018**, *15*, 617-638.
[4] M. L. Merchant, I. M. Rood, J. K. J. Deegens, J. B. Klein, *Nat. Rev. Nephrol.* **2017**, *13*, 731-749.
[5] a) N. Kosaka, H. Iguchi, T. Ochiya, *Cancer Sci.* **2010**, *101*, 2087-2092; b) E. Ozkumur, A. M. Shah, J. C. Ciciliano, B. L. Emmink, D. T. Miyamoto, E. Brachtel, M. Yu, P. I. Chen, B. Morgan, J. Trautwein, A. Kimura, S. Sengupta, S. L. Stott, N. M. Karabacak, T. A. Barber, J. R. Walsh, K. Smith, P. S. Spuhler, J. P. Sullivan, R. J. Lee, D. T. Ting, X. Luo, A. T. Shaw, A. Bardia, L. V. Sequist, D. N. Louis, S. Maheswaran, R. Kapur, D. A. Haber, M. Toner, *Sci. Transl. Med.* **2013**, *5,* 197ra47.
[6] G. Chen, A. Huang, W. Zhang, G. Zhang, M. Wu, W. Xu, Z. Yu, J. Yang, B. Wang, H. Sun, H. Xia, Q. Man, W. Zhong, L. Antelo, B. Wu, X. Xiong, X. Liu, L. Guan, T. Li, S. Liu, R. Yang, Y. Lu, L. Dong, S. McGettigan, R. Somasundaram, R. Radhakrishnan, G. Mills, Y. Lu, J. Kim, Y. Chen, H. Dong, Y. Zhao, G. C. Karakousis, T. C. Mitchell, L. M. Schuchter, M. Herlyn, E. J. Wherry, X. Xu, W. Guo, *Nature* **2018**, *560*, 382-386.
[7] a) X. Doldan, P. Fagundez, A. Cayota, J. Laiz, J. P. Tosar, *Anal. Chem.* **2016**, *88*, 10466-10473; b) S. Jeong, J. Park, D. Pathania, C. M. Castro, R. Weissleder, H. Lee, *ACS Nano* **2016**, *10*, 1802-1809; c) S. Wang, L. Zhang, S. Wan, S. Cansiz, C. Cui, Y. Liu, R. Cai, C. Hong, I. Teng, M. Shi, Y. Wu, Y. Dong, W. Tan, *ACS Nano* **2017**, *11*, 3943-3949.
[8] a) K. Hsieh, B. S. Ferguson, M. Eisenstein, K. W. Plaxco, H. T. Soh, *Acc. Chem. Res.* **2015**, *48*, 911-920; b) P. Wie, Z. Ning, S. Ye, L. Sun, F. Yang, K. Wong, D. Westerdahl, P. K. K. Louie, *Sensors* **2018**, *18,* 59.
(9) S. Zong, L. Wang, C. Chen, J. Lu, D. Zhu, Y. Zhang, Z. Wang, Y. Cui, *Anal. Methods* **2016**, *8*, 5001-5008.
[10] a) H. Im, H. Shao, Y. I. Park, V. M. Peterson, C. M. Castro, R. Weissleder, H. Lee, *Nat. Biotechnol.* **2014**, *32*, 490-495; b) Y. Jiang, M. Shi, Y. Liu, S. Wan, C. Cui, L. Zhang, W. Tan, *Angew. Chem., Int. Ed.* **2017**, *56*, 11916-11920; *Angew. Chem.* **2017**, *129*, 12078–12082 c) Y. Xia, M. Liu, L. Wang, A. Yan, W. He, M. Chen, J. Lan, J. Xu, L. Guan, J. Chen, *Biosens. Bioelectron.* **2017**, *92*, 8-15.
[11] a) J. M. Lewis, A. D. Vyas, Y. Q. Qiu, K. S. Messer, R. White, M. J. Heller, *ACS Nano* **2018**, *12*, 3311-3320; b) K. Mori, M. Hirase, T. Morishige, E. Takano, H. Sunayama, Y. Kitayama, S. Inubushi, R. Sasaki, M. Yashiro, T. Takeuchi, *Angew. Chem., Int. Ed.* **2019**, *58*, 1612-1615; *Angew. Chem.* **2019**, *131*, 1626-1629.
[12] N. C. Whittington; S. Wray, *Curr. Protoc. Neurosci.* **2017**, *81*, 2.28.21-22.28.12.
[13] a) J. Li, K. Pu, *Chem. Soc. Rev.* **2019**, *48*, 38-71; b) C. Zhu, L. Liu, Q. Yang, F. Lv, S. Wang, *Chem. Rev.* **2012**, *112*, 4687-4735; c) Y. Jiang, K. Pu, *Acc. Chem. Res.* **2018**, *51*, 1840-1849; d) C. F. Wu, D. T. Chiu, *Angew. Chem., Int. Ed.* **2013**, *52*, 3086-3109; *Angew. Chem.* **2013**, *125*, 3164–3190; e) L. Feng, C. Zhu, H. Yuan, L. Liu, F Lv and S. Wang, *Chem. Soc. Rev.* **2013**,*42*, 6620-6633; f) J. Wang, F. Lv, L. Liu, Y. Ma and S. Wang, *Coord. Chem. Rev.* **2018**, *354*, 135-154; g) X. Zhen, C. XIe, Y. Jiang, X Ai, B Xing, K. Pu, *Nano Lett.* **2018**, *18*, 1498-1505.
[14] a) Q. Miao, C. Xie, X. Zhen, Y. Lyu, H. Duan, X. Liu; J. V. Jokerst; K. Pu, *Nat. Biotechnol.* **2017**, *35*, 1102-1110; b) C. Xie, X. Zhen, Q. Miao, Y. Lyu, K. Pu, *Adv. Mater.* **2018**, *30*, 1801331; c) D. Cui, C. Xie, J. Li, Y. Lyu, K. Pu, *Adv. Healthc. Mater.* **2018**, *7*, 1800329; d) C. Xie, Y. Lyu, X. Zhen, Q. Miao, K. Pu, *ACS Appl. Bio Mater.* **2018**, *1*, 1147-1153: e) Q. Miao, K. Pu. *Adv. Mater.* **2018**, 30, 1801778; f) X. Zhen, C. Xie, K. Pu. *Angew. Chem. Int. Ed.* **2018**, 57, 3938-3942; *Angew. Chem.* **2018**, *130*, 4002-4006; g) Y. Jiang, J. Li, X. Zhen, K. Pu, *Adv. Mater.* **2018**, *30*, 1705980.
[15] F. Properzi, M. Logozzi, S. Fais, *Biomark. Med.* **2013**, *7*, 769-778.
[16] C. M. Klinge, B. N. Radde, Y. Imbert-Fernandez, Y. Teng, M. M. Ivanova, S. M. Abner, A. L. Martin, *Mol. Cancer Ther.* **2011**, *10*, 2062-2071.

COMMUNICATION

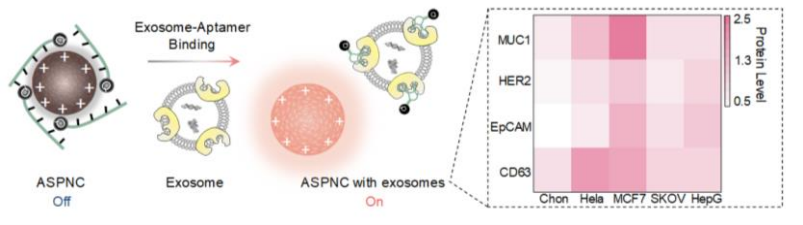

*Yan Lyu, Dong Cui, Jiaguo Huang, Wenxuan Fan, Yansong Miao and Kanyi Pu**

Page No. – Page No.

Near-infrared Afterglow Semiconducting Nano-polycomplexes for Multiplex Differentiation of Cancer Exosomes

The first luminescent turn-on nanosensor that bypasses real-time light excitation for multiplex differentiation of cancer exosomes is reported, which is composed of a near-infrared (NIR) semiconducting polyelectrolyte (ASPN) electrostatically complexed with a quencher-tagged aptamer.